



Supplementary Information for

Theory of mechano-chemical patterning in biphasic biological tissues

P. Recho, A. Hallou and E. Hannezo

Emails: pierre.recho@univ-grenoble-alpes.fr or ah691@cam.ac.uk or edouard.hannezo@ist.ac.at

This PDF file includes:

Supplementary text
Figs. S1 to S5
References for SI reference citations

Supporting Information Text

1. Results

A. Derivation of the model.

A.1. Tissue spatial organisation. As sketched in Fig. 1A of main text, we model multicellular tissues as biphasic porous media, with a first phase consisting in a three-dimensional elastic meshwork made of interconnected cells, and a second phase being made up of aqueous extracellular fluid permeating in-between cells. The typical lengthscale of the whole tissue is l . Cells, compartmentalized by their plasma membrane have a typical diameter l_c and the average intercellular or interstitial space has a characteristic size l_i . Typically, these three lengthscales are well-separated such that:

$$l \gg l_c \gg l_i.$$

We adopt a continuum description of the tissue where all physical quantities are averaged over a representative volume element (RVE) of intermediate size $l \gg l_r \gg l_c$ at which the system can be coarse-grained (1, 2). At that scale, we introduce the space coordinate $\vec{r} \in \Omega$, where Ω is the domain occupied by the whole tissue, and t denotes the time coordinate.

A.2. Derivation of the biphasic model. Although we only consider a biphasic media in the main text of this manuscript, a more complete version of the model would introduce three volume fractions within the tissue: $\phi_s(\vec{r}, t)$ the volume occupied by the skeletal meshwork of cells divided by the volume of the RVE, $\phi_c(\vec{r}, t)$ the volume of fluid contained within cell membranes divided by the volume of the RVE and $\phi_e(\vec{r}, t)$ the volume occupied by interstitial fluid divided again by the RVE. In the following, we provide a rationale and orders of magnitude for considering only two phases in the main text.

As a consequence of volume conservation, we have here:

$$\phi_s + \phi_c + \phi_e = 1.$$

A difference with the simple biphasic model is that there are here three velocities associated with each of the phases, v_s , v_c and v_e . Importantly, although it could be thought that fluid is only exchanged between cells and extracellular medium (meaning that $v_c = v_s$ *i.e.* solid phase and intracellular fluid are advected together), this is not the case, as gap junctions allow for direct cell-cell communication and fluid exchange (which means that in a triphasic model there can be non-zero v_c with vanishing v_s). This point is important to consider when writing intracellular morphogen conservation equations, as v_s would be included in an advective term, whereas v_c would not, as most morphogens are too large to be transported through gap junctions. In order to simplify the description of the system, we make two important assumptions relative to the cellular meshwork phase. First, as both cells and extracellular space are mostly composed of fluid, we neglect the volume fraction occupied by the cellular meshwork such that $\phi_c \stackrel{\text{def}}{=} \phi$ and $\phi_e \simeq 1 - \phi$. Then, we assume that the velocity of cells moving in the tissue is very slow compared to the velocity of fluid flows in the extracellular space and from cell to cell. Thus, the present study focuses on cell specification patterns considering that the evolution of the tissue topology is quasi-static. To make this approximation clearer, we provide below (Section A.3) simple physical estimates showing that the characteristic timescales associated with tissue remodelling processes, such as cell proliferation and active cell motility, can be larger by an order of magnitude than fluid circulation inside the tissue.

In Section I, we also show how the theory can be extended to account for large scale tissue remodelling occurring during embryonic development when tissue topology is changing on a timescale similar to that of fluid flows inside the tissue.

A.3. Fluid re-circulation vs tissue remodelling. Large scale advective flows of extracellular fluid must be compensated by some recirculation of fluid ensuring global volume conservation (except if there are exchanges with other tissues, which we do not consider here for the sake of simplicity). We first consider the possibility that this re-circulation occurs through intracellular fluid flows, and calculate the time scales associated with this process. In general, there are three characteristic timescales associated with fluid circulation inside a multicellular tissue: τ_i for fluid flows inside the interstitial space, τ_c for fluid flows from one cell to the other through gap junctions, and finally τ for the exchanges of fluid between cells and the extracellular fluid through aquaporins.

As we demonstrate in Section A.7 using a poroelastic model of multicellular tissues, τ_i and τ_c can be interpreted as diffusive timescales and take the form,

$$\tau_i = \eta l_p^2 / (\kappa K) \text{ and } \tau_c = \eta l_p^2 / (\kappa_c K)$$

where $\eta \approx 10^{-3}$ Pa.s is the viscosity of the aqueous cytosolic fluid (3, 4), $K \approx 10^4$ Pa is the drained elastic modulus of the tissue (5), $l_p \approx 10^{-4}$ m the characteristic size of multicellular patterns in the tissue. κ and κ_c (expressed in m^2) are the effective interstitial and cell to cell water permeabilities. In agreement with the typical timescales involved in cell volume changes following an osmotic perturbation (6), we estimate that $\tau \approx 10^2 - 10^3$ s. In the main text, based on typical tissue interstitial sizes and packing fractions, we estimate the interstitial permeability $\kappa \approx 10^{-15} - 10^{-19}$ m^2 leading to $\tau_i \approx 1 - 10^4$ s. We note that this estimate is one of the coarsest one in the model, as the packing fraction of multicellular tissues can vary widely between tissues, developmental stages and species.

Finally, the cell-cell permeability relies on gap junctions which are highly specialized membrane structures made of clusters of transmembrane protein channels named connexons and which connect together the cytoplasm of neighbouring cells (7). The

ensuing permeability can be estimated in applying the Darcy-Weisbach equation to a parallel array of connexons mediating the cell to cell fluid flux:

$$\kappa_c = \frac{d^2}{32} \left(1 + n \frac{d^2}{\delta l_c} \right) \approx 3 \times 10^{-18} \text{ m}^2$$

taking, $l_c \approx 10^{-5}$ m the diameter of a cell, $n \approx 10^5$ as the average number of connexons at a cell-cell interface (8–11), $d \approx 3 \times 10^{-9}$ m (7) as the typical diameter of a connexon and $\delta \approx 10^{-8}$ m as its length (7, 12). The coefficient 32 is the friction factor for a laminar flow (13). Interestingly, this simple theoretical estimate of κ_c is in line with direct experimental measurements using fluorescent dyes injected in the cytoplasm of cells in epithelial cell monolayers (14, 15). Eventually, this yields to an estimate of $\tau_c \approx 4 \times 10^2$ s.

Next, we compare these timescales for direct cell-cell fluid re-circulation to the timescale associated with tissue remodelling. Indeed, an alternative to enforce global volume conservation given extracellular fluid flows would be to have a counter-flow of the cellular meshwork. Typically, this would be very slow, as the viscosity of multicellular tissues is very high. Such a timescale has been estimated from rheological measurements made on various multicellular tissues (16, 17) and is typically $\tau_r \approx 10^4$ s, associated with slow tissue re-arrangement and remodelling. This slow timescale is consistent with the observed timescales for cell division and cell motility, which have been both noted as major sources of tissue remodelling (18). The typical timescale of cell division in embryonic tissues is $\tau_d \approx 10^4 - 10^5$ s. The characteristic velocity of a cell moving within such a tissue is $v_m \approx 10^{-9}$ m.s⁻¹. Over the characteristic size $l_p \approx 10^{-4}$ m of tissue patterning, this leads to a typical timescale for motility-driven remodelling of $\tau_m \approx 10^5$ s.

In the end, it appears that all three timescales associated with fluid flows are either slightly or much smaller compared to the timescale associated with tissue remodelling and cellular flows. Therefore, in our model, we shall consider tissue remodelling as a quasi-static process and assume a fixed tissue structure during the faster fluid exchanges in-between cells or between cells and extracellular fluid. A more complete description incorporating these effects and which does not make such a simplifying assumption is presented in Section I. This is motivated by the fact that in some biological systems, during early embryogenesis, cell division could be faster than our estimate, closer to $\tau_d \approx 10^3$ s. In this situation, plastic re-arrangements of the tissue could be potentially more important and play a role in the patterning instabilities we describe.

A.4. Fluid conservation. As fluid can be exchanged between cells and between cells and extracellular medium, we can write, assuming fluid incompressibility, the following mass balance relations:

$$\begin{aligned} \partial_t \phi + \nabla \cdot (\phi v_c) &= S \\ \partial_t (1 - \phi) + \nabla \cdot ((1 - \phi) v_e) &= -S \end{aligned} \quad [1]$$

where $v_{c,e}(\vec{r}, t)$ are velocities associated with fluid flows respectively inside and outside the cells. It should be noted that because these equations are defined at a coarse-grained level, v_c refers to fluid flowing directly from one cell to the other, which occurs in multicellular tissues via gap junctions, as discussed in the previous section. Gap junctions have been well-characterised as key regulators of cell-cell coupling, allowing in addition of fluid transport, the movement of inorganic ions and small water-soluble molecules from the cytoplasm of one cell to the other (19). Nevertheless, most morphogens cannot cross through gap junctions, as they are proteins whose size exceeds by far the diameter of connexons lumen (7, 12). Crucially, in our model, this means that although extracellular flows v_e can advect morphogens, this is not the case of intercellular flows v_c . This allows advection to concentrate morphogens locally, as they do not participate in fluid re-circulation.

Summing up the two previous mass balance equations, we obtain $\nabla \cdot (\phi v_c + (1 - \phi) v_e) = 0$ which is generally satisfied if:

$$v_c = -\frac{1 - \phi}{\phi} v_e.$$

As ϕ is usually rather close to one, the cell to cell fluid velocity v_c is thus expected to be much smaller than the velocity of fluid flows developing in the extracellular space in-between cells v_e . However, in spite of taking relatively low values, v_c should not be neglected, as it is central for the model consistency and in enforcing volume conservation in the system. We note here that although the cell volume fraction ϕ is close to one in various multicellular tissues, our theory does not depend on that assumption, and can in principle accommodate values of ϕ very different from one.

The source term S , on the right-hand side of Eq. 1, originates both in the genetically controlled transport of water between cells and extracellular medium, which occurs through specific transmembrane proteins named aquaporins (20, 21) and on the balance between cell division and apoptosis regulating the number of cells in a RVE. In absence of spatial fluid flows in interstitial spaces or at tissue boundaries, we have:

$$S = \partial_t \phi = \partial_t (N_c V_c) / V_r$$

where N_c is the number of cells in a RVE, V_c the volume of a single cell and V_r the volume of an RVE. When submitted to an external osmotic shock or mechanical load, the volume of cells transiently increases or decreases prior to relaxing to an homeostatic volume V_h . Considering an exponential relaxation, we can write:

$$\partial_t V_c = \frac{V_h - V_c}{\tau}$$

where τ is the typical timescale associated with a regulatory response to cell volume changes. This time scale can be estimated to be of the order of $\sim 10^2 - 10^3$ s in the case of an osmotic shock (6).

In our model, as discussed with the orders of magnitude provided in Section A.3, the tissue topology is taken to be fixed and we thus neglect the variations of N_c due to cell division and cell loss. However, we present below a more general argument and show that these phenomena does not impact the expression of the term S in Eq. (1). This argument will be also used to justify the general model presented in Section I where tissue topology becomes dynamic thanks to cell motility and cell turnover.

The simplest evolution law for N_c is given by $\partial_t N_c = s_d - N_c k_a$, where s_d accounts for cell division and k_a is the cell loss rate. This law can be rewritten as

$$\partial_t N_c = \frac{N_h - N_c}{\tau_d},$$

where $\tau_d = k_a^{-1}$ is the typical duration of a cell cycle of the order of $\sim 10^4 - 10^5$ s (during chick limb bud patterning this time is about $10 h = 3.6 \times 10^4$ s) and $N_h = s_d \tau_d$ is the equilibrium number of cells when cell division balances cell loss. Defining $\phi_h = N_h V_h / V_r$ the homeostatic volume fraction of cells and δV and δN some initial perturbations from the homeostatic state, we obtain:

$$S = \frac{\tau + \tau_d}{\tau \tau_d} (\phi_h - \phi) + \phi_h \left(\frac{\delta V}{V_h} \tau_d^{-1} e^{-t/\tau} + \frac{\delta N}{N_h} \tau^{-1} e^{-t/\tau_d} \right).$$

Considering typical timescales such that $t \gg \tau$ and as $\tau_d \gg \tau$, the first term dominates the last expression and we finally obtain $S = (\phi_h - \phi)/\tau$.

In agreement with the fact that cell fate decisions are usually accompanied by modifications of the cell cycle and cell morphology, including cell volume changes, we suppose that ϕ_h depends on the concentrations of morphogens (22–24). Indeed, most of the known morphogens are in fact growth factors which regulate both cell differentiation but also cell growth and cell division (25–28). We can thus write the source term of the conservation equation as:

$$S = \frac{\phi_h(A_i, I_i) - \phi}{\tau}$$

where $\phi_h(A_i, I_i)$ is the cell volume fraction with cells in their homeostatic volume state.

As mentioned above, it should be noted for the sake of completeness that we have assumed here a closed-system, where no fluid is exchanged between the tissue and the rest of the organism. Relaxing this assumption would be equivalent to adding another source term, S_b , in the conservation equation for $1 - \phi$ (see Eq. 1), without adding it to the conservation equation for ϕ . This would be an alternative to intracellular fluid re-circulation to allow for the existence of non-zero steady state fluid flows in the tissue.

A.5. Morphogen conservation outside cells. Conservation equations for morphogens in the extracellular space are given by:

$$\begin{aligned} \partial_t((1 - \phi)A_e) + \nabla \cdot (A_e(1 - \phi)v_e - D\nabla A_e) &= -\gamma_A A_e + \lambda_A A_i \\ \partial_t((1 - \phi)I_e) + \nabla \cdot (I_e(1 - \phi)v_e - D\nabla I_e) &= -\gamma_I I_e + \lambda_I I_i \end{aligned} \quad [2]$$

where $\gamma_{A,I}$ and $\lambda_{A,I}$ are respectively the import and export rates of morphogens through some specific channels and pumps, and D is the common global diffusion coefficient of both morphogens in the intercellular space. D do not refer to a molecular diffusion coefficient but to an homogenized quantity over a RVE.

A.6. Morphogen conservation inside cells. Conservation equations for morphogens inside cells read:

$$\begin{aligned} \partial_t(\phi A_i) &= f(A_i, I_i) + \gamma_A A_e - \lambda_A A_i \\ \partial_t(\phi I_i) &= g(A_i, I_i) + \gamma_I I_e - \lambda_I I_i \end{aligned} \quad [3]$$

where f and g are the morphogens turnover rates, non-linear functions of morphogen concentrations describing their production and degradation by cells. Note here, that these reaction terms could also be a function of extracellular morphogen concentrations, describing a biological situation where signaling at the membrane also directs internal morphogen production and degradation. While such an addition would be biologically relevant, it nevertheless does not alter the mathematical formulation of our final model Eq. (10) as explained in Section C.

The vector field $[f, g]$ is assumed to have a single stable equilibrium point (A_i^*, I_i^*) such that $f(A_i^*, I_i^*) = g(A_i^*, I_i^*) = 0$ and $\det \mathbb{J} > 0$ and $\text{tr } \mathbb{J} < 0$ such that the eigenvalues of the jacobian matrix

$$\mathbb{J} = \begin{pmatrix} \partial_{A_i^*} f & \partial_{I_i^*} f \\ \partial_{A_i^*} g & \partial_{I_i^*} g \end{pmatrix}$$

are negative. Here, we do not consider the complex case where morphogens can undergo transitions between various stable chemical states.

Contrary to Eq. (2), advective terms are absent in Eq. (3), as known morphogens are too large to be transported through gap junctions (7, 12). Indeed, because of this impossibility of direct cell to cell transport of morphogens, advective terms would equate the transport terms $\nabla(\phi A_i v_s)$ and $\nabla(\phi I_i v_s)$, where $v_s(\vec{r}, t)$ is the cellular meshwork velocity, which we neglect here in ignoring cellular motion. Such an assumption is critically discussed in Section I.

A.7. Effective mechanical behaviour of the tissue. To complete the model described by Eqs. (1,2,3), we need to relate the interstitial fluid velocity, v_e , with the cell volume fraction ϕ . Such a link is modelled using the classical poroelastic theory (29, 30).

When biochemical reactions involving morphogens are at equilibrium, Eq. (1) has an homogeneous solution given by:

$$v_e = 0 \text{ and } \phi \stackrel{\text{def}}{=} \phi^* = \phi_h(A_i^*, I_i^*)$$

This state of the tissue constitutes a ‘‘reference configuration’’ where the deformation of the multicellular network is considered to be null. Supposing small variations from this reference state, we can write an effective quadratic mechanical free energy for the cellular network, F , coupling the tensorial infinitesimal strain \mathbb{E} with porosity variations $\delta\phi = \phi - \phi^*$. The free energy of a poroelastic tissue reads:

$$F = G\mathbb{E} : \mathbb{E} + \left(\frac{K_u}{2} - \frac{G}{3}\right) [\text{tr}(\mathbb{E})]^2 + \frac{K_u - K}{\alpha} \text{tr}(\mathbb{E})\delta\phi + \frac{K_u - K}{2\alpha^2} [\delta\phi]^2$$

where G is the shear modulus of the tissue, K is its drained modulus, K_u its undrained modulus and α its Biot coefficient.

We derive the non-dissipative mechanical stress in the tissue, σ , and the interstitial fluid pressure p by differentiation of the free energy:

$$\begin{aligned} \sigma &= \partial_e F = 2G\mathbb{E} + \left(K - \frac{2G}{3}\right) \text{tr}(\mathbb{E})\mathbb{1} - \alpha p\mathbb{1} \\ p &= -\partial_{\delta\phi} F = -\frac{K_u - K}{\alpha} \text{tr}(\mathbb{E}) - \frac{K_u - K}{\alpha^2} \delta\phi, \end{aligned} \quad [4]$$

where $\mathbb{1}$ denotes the identity matrix. In this classical theory, mechanical energy dissipation is assumed to happen mainly through viscous friction of the extra-cellular fluid permeating in between the cells and is described using Darcy’s law:

$$(1 - \phi)v_e = -\frac{\kappa}{\eta} \nabla p,$$

as, again, we neglect v_s in this framework, but this time as compared to the extracellular fluid velocity v_e . The tissue permeability is denoted κ ($[\text{m}^2]$) and η is the viscosity of the permeating aqueous fluid.

Finally, force balance within the tissue implies that $\nabla \cdot \sigma = 0$, which using the first constitutive relation Eq. (4) leads to:

$$2G\nabla \cdot \mathbb{E} + \left(K - \frac{2G}{3}\right) \nabla \text{tr}(\mathbb{E}) = \alpha \nabla p.$$

Coupling that last equation with the second equation of Eq. (4) and assuming, in line with the typical orders of magnitude for biological tissues (31, 32) that

$$K_u \gg K \gg G \text{ and } \alpha \simeq 1,$$

we obtain the simple relation:

$$(1 - \phi)v_e = -\frac{\kappa}{\eta} \nabla p = \frac{K\kappa}{\eta} \nabla \phi, \quad [5]$$

relating v_e and ϕ where we can introduce the hydrodynamic diffusion coefficient of the extracellular fluid through the tissue $D_m = K\kappa/\eta$, which is, as explained in the main text, a driving force of the instability, counter-acting morphogen Fickian diffusion which acts as a resisting force.

B. Model of an active biphasic tissue. Coupling Eqs. (1,2,3,5), the full set of equations describing the chemo-mechanical behaviour of an active biphasic multicellular tissue can be written as:

$$\begin{aligned} \partial_t(\phi A_i) &= f(A_i, I_i) + \gamma_A A_e - \lambda_A A_i \\ \partial_t(\phi I_i) &= g(A_i, I_i) + \gamma_I I_e - \lambda_I I_i \\ \partial_t((1 - \phi)A_e) + \nabla \cdot (A_e D_m \nabla \phi - D \nabla A_e) &= -\gamma_A A_e + \lambda_A A_i \\ \partial_t((1 - \phi)I_e) + \nabla \cdot (I_e D_m \nabla \phi - D \nabla I_e) &= -\gamma_I I_e + \lambda_I I_i \\ \partial_t \phi - \nabla \cdot (D_m \nabla \phi) &= \frac{\phi_h(A_i, I_i) - \phi}{\tau}. \end{aligned}$$

This system of coupled equations can also be written in a more compact matrix form:

$$\begin{aligned} \partial_t(\phi \underline{X}_i) &= \underline{F}(\underline{X}_i) + \mathbb{F} \underline{X}_e - \mathbb{A} \underline{X}_i \\ \partial_t((1 - \phi) \underline{X}_e) + \nabla \cdot (D_m \nabla \phi \underline{X}_e - D \nabla \underline{X}_e) &= -\mathbb{F} \underline{X}_e + \mathbb{A} \underline{X}_i \\ \partial_t \phi - \nabla \cdot (D_m \nabla \phi) &= \frac{\phi_h(\underline{X}_i) - \phi}{\tau}, \end{aligned} \quad [6]$$

where $\underline{X}_{i,e} = (A_{i,e}, I_{i,e})$ are the morphogen concentration vectors, $\underline{F}(\underline{X}_i) = (f(A_i, I_i), g(A_i, I_i))$ is the morphogen turnover rates vector, and

$$\mathbb{A} = \begin{pmatrix} \lambda_A & 0 \\ 0 & \lambda_I \end{pmatrix} \text{ and } \mathbb{F} = \begin{pmatrix} \gamma_A & 0 \\ 0 & \gamma_I \end{pmatrix}$$

are the diagonal matrices of transmembrane import and export rates of morphogens.

The model has as a single homogeneous steady state solution given by:

$$\phi \equiv \phi^*, \underline{X}_i = \underline{X}_i^* \text{ and } \underline{X}_e = \mathbb{K} \underline{X}_i^* \quad [7]$$

where $\mathbb{K} = \mathbb{A}\Gamma^{-1}$ is the matrix of the transmembrane transport equilibrium constants.

To investigate the stability of this solution and fully specify the problem, we need, in addition of Eq. (6), to define initial and boundary conditions. The initial condition is typically chosen as a random perturbation of the homogeneous solution Eq. (7). For the boundary conditions on the frontier $\partial\Omega$ of the domain Ω , we impose a no-flux of fluid and morphogens:

$$\nabla \underline{X}_e \cdot n|_{\partial\Omega} = \nabla \phi \cdot n|_{\partial\Omega} = 0,$$

where n is the outward normal of Ω . Such boundary conditions are natural as they correspond to an isolated system and we wish to consider endogenous pattern formation that are not externally driven.

Eventually, we also need to specify the non-linear function f, g and ϕ_h as a function of the internal morphogens concentrations. For f and g , we will essentially consider two cases in this paper:

For Fig. 2 of the main text, we use the classical activator-inhibitor Gierer-Meinhardt scheme (33–35) (see section "Turing-Keller-Segel instabilities" in the main text):

$$\begin{aligned} f(A_i, I_i) &= \rho \frac{A_i^2}{I_i^2} - \frac{A_i}{\tau_A} \\ g(A_i, I_i) &= \rho A_i^2 - \frac{I_i}{\tau_I}, \end{aligned} \quad [8]$$

where ρ is the rate of activation and inhibition and $\tau_{A,I}$ the timescales of degradation of A and I . Within this scheme, $A_i^* = \tau_A/\tau_I$ and $I_i^* = \rho\tau_A^2/\tau_I$.

For Fig. 4 of the main text, to illustrate the instability induced by the hydrodynamic cross-diffusion (see section "Cross-diffusion Turing instabilities" in the main text), we construct a very simple inhibitor-inhibitor scheme where:

$$\begin{aligned} f(A_i, I_i) &= -\frac{(A_i - A_i^*)}{\tau_A} - \frac{(I_i - I_i^*)}{\tau_I} + \Psi(A_i, I_i) \\ g(A_i, I_i) &= -\frac{(A_i - A_i^*)}{\tau_I} - \frac{(I_i - I_i^*)}{\tau_A} + \Psi(A_i, I_i), \end{aligned}$$

and,

$$\Psi(A_i, I_i) = -\beta \left[\left(\frac{A_i - A_i^*}{A_i^*} \right)^2 + \left(\frac{I_i - I_i^*}{A_i^*} \right)^2 \right] H(A_i - A_{\min}) H(I_i - I_{\min})$$

is a non-linear function chosen to ensure that A_i and I_i remain bounded and positive (H denotes the Heaviside function). Parameters used for the figure numerical simulation are $\beta K_A \tau_A = 1$, $A_{\min}/A_i^* = I_{\min}/I_i^* = 1$ and $l_A/l = 0.1$.

Generically, $\phi_h(A_i, I_i)$ could be a rather complex function. However, for a linear stability analysis of patterning instabilities, we can restrict its functional form to a first-order linear expansion of the cell volume fraction around the reference state:

$$\phi_h(A_i, I_i) = \phi^* + \chi_A (A_i - A_i^*)/A_i^* + \chi_I (I_i - I_i^*)/I_i^* \quad [9]$$

The term ϕ^* accounts for mechanisms controlling cell volume and proliferation that are independent of morphogens levels, such as mechanical stress caused by active cell contractility (36), osmotic effects due to passive water flows through aquaporins (20, 21) and ions efflux/influx by transmembrane ion channels and pumps (6). The $\chi_{A,I}$ terms account for the sensitivity of homeostatic cell volume fraction to intracellular morphogens concentrations and thus depend on how morphogens regulate both the volume of individual cells but also their proliferation. We also note that although this linear expansion is valid to study the onset of the instability, this does not constrain ϕ to be bound between 0 and 1, which is required from a physical perspective, and arises from non-linear terms. This becomes important for numerical simulations, where non-linear terms are crucial to stabilize the amplitude of the instability, so we chose for all numerical integrations:

$$\phi_h(A_i, I_i) = \frac{\phi^* \left(\tanh \left(\frac{\chi_A (A_i - A_i^*)/A_i^* + \chi_I (I_i - I_i^*)/I_i^*}{2(1 - \phi^*)\phi^*} \right) + 1 \right)}{(2\phi^* - 1) \tanh \left(\frac{\chi_A (A_i - A_i^*)/A_i^* + \chi_I (I_i - I_i^*)/I_i^*}{2(1 - \phi^*)\phi^*} \right) + 1},$$

which is compatible with the linear approximation mentioned above.

C. Simplified model. To achieve mathematical tractability and discuss the solutions of the model in a biophysically relevant context, it is possible to reduce Eq. (6) by assuming that the import rates $\Gamma \gg \mathbb{A} \gg \mathbb{J}$ are much larger than the export rates, such that $\mathbb{K} \ll 1$ is small and that the import/export dynamics is faster than morphogens turnover. From a biological standpoint (see also Section G.3 for further details) $\Gamma, \mathbb{A} \approx 10^{-2} \text{ s}^{-1} \gg \mathbb{J} \approx 10^{-4} \text{ s}^{-1}$, (37) and we explain in Section F why we additionally consider the limit $\mathbb{K} \ll 1$. Note however that we demonstrate in Section G.1 that the Keller-Segel instability that we disclose in the single morphogen case does not depend on the simplifying double limit considered in this Section.

When $\Gamma \gg \mathbb{A} \gg \mathbb{J}$, morphogen import and export almost balance each other such that $\underline{X}_e \simeq \mathbb{K}\underline{X}_i$. As a result the external concentrations of morphogens are small compared to the internal ones. However, exchange terms in Eq. (6) remain finite because $\Gamma^{-1}(\underline{X}_e - \mathbb{K}\underline{X}_i)$ is an indeterminate product between a large quantity (Γ^{-1}) and a small one ($\underline{X}_e - \mathbb{K}\underline{X}_i$). To resolve this indeterminate form, we sum up the first and second equations of Eq. (6) such that the exchange terms exactly cancel out each other and, as $\underline{X}_e \simeq \mathbb{K}\underline{X}_i$, we obtain a closed system for the internal morphogens concentration:

$$\begin{aligned} \partial_t(\phi \underline{X}_i) + \nabla \cdot (D_m \mathbb{K} \nabla \phi \underline{X}_i - \mathbb{K} D \nabla \underline{X}_i) &= F(\underline{X}_i) \\ \tau \partial_t \phi - \nabla \cdot (\tau D_m \nabla \phi) &= \phi_h(\underline{X}_i) - \phi. \end{aligned}$$

For such a system to be non-trivial, we assume that both $D_m \mathbb{K}$ and $D \mathbb{K}$ remain finite. This implies that the diffusion D_m is large and for $l_m = \sqrt{D_m \tau}$ to remain finite as well, we also need to assume that $\tau \sim \tau_A K_A \ll 1$ is small. As a result, the cell volume fraction relaxes infinitely fast and we finally obtain the simplified model:

$$\begin{aligned} \partial_t(\phi \underline{X}_i) + \nabla \cdot (D_m \mathbb{K} \nabla \phi \underline{X}_i - \mathbb{K} D \nabla \underline{X}_i) &= \underline{F}(\underline{X}_i) \\ -l_m^2 \nabla^2 \phi + \phi &= \phi_h(\underline{X}_i), \end{aligned} \quad [10]$$

which couples a reaction-advection-diffusion equation for the morphogens levels with an elliptic equation controlling the drift as a function of the morphogen levels. Interestingly, the mathematical structure of this model is reminiscent of some previous models which have been proposed in the completely different context of cytoskeleton self-organisation (38).

At this stage, we note that the robustness of the model with respect to two hypothesis can be demonstrated. In Eq. (6), we can add to the second equation a degradation term for the external morphogen concentrations $-\Gamma_{\text{ext}} \underline{X}_e$ and we can also suppose that, in the third equation $\phi(\underline{X}_i, \underline{X}_e)$ also depends on \underline{X}_e . As $\underline{X}_e = \mathbb{K} \underline{X}_i$, this will not change the form of Eq. (10) but only effectively rescale the expressions of \underline{F} and ϕ_h .

Importantly, when $\chi_{A,I} = 0$ (no sensitivity of the volume fraction on morphogen concentrations), the second equation uncouples from the first one such that $\phi \equiv \phi^*$ and Eq. (10) reduces to the classical Turing case:

$$\phi^* \partial_t \underline{X}_i - \mathbb{K} D \nabla^2 \underline{X}_i = \underline{F}(\underline{X}_i)$$

which is fully studied in (39) with the only difference that here the global diffusion of morphogens is now rescaled by the transmembrane transport equilibrium constants (see section "Orders of magnitude on morphogen transport" in the main text).

D. Stability analysis of the simplified model. We are now interested in determining if we can obtain a stationary spatial pattern for morphogens concentrations in perturbing the system Eq. (10) in the vicinity of its homogeneous equilibrium state. To do so, we write:

$$\underline{X}_i = \underline{X}_i^* + \epsilon \delta \underline{X}_i \text{ and } \phi = \phi^* + \epsilon \delta \phi$$

where $\epsilon \ll 1$, and we obtain at the first order in ϵ :

$$\begin{aligned} \underline{X}_i^* \partial_t \delta \phi + \phi^* \partial_t \delta \underline{X}_i + D_m \mathbb{K} \underline{X}_i^* \nabla^2 \delta \phi - D \mathbb{K} \nabla^2 \delta \underline{X}_i &= \mathbb{J} \delta \underline{X}_i \\ -l_m^2 \nabla^2 \delta \phi + \delta \phi &= \nabla_{\underline{X}_i} \phi_h|_{\underline{X}_i^*} \cdot \delta \underline{X}_i. \end{aligned}$$

We now introduce the sets of eigenvalues $\{\lambda_k\}_{k \geq 1}$ and eigenvectors $\{U_k(\vec{r})\}_{k \geq 1}$ of the minus Laplace operator defined by the problem:

$$\begin{cases} -\nabla^2 U_k = \lambda_k U_k \\ \nabla U_k \cdot n|_{\partial \Omega} = 0. \end{cases} \quad [11]$$

By classical theorems (39), $\{\lambda_k\}$ is a countable set of positive and increasing values, and $\{U_k\}$ forms a basis on which we can project the solutions of the linearised system :

$$\delta \underline{X}_i(\vec{r}, t) = \sum_{k=1}^{\infty} \underline{X}_i^k U_k(\vec{r}) \exp(\omega_k t),$$

where ω_k is the growth rate associated to the k^{th} growth mode. For example, when Ω is a one dimensional segment of size l we have $\lambda_k = (\pi k/l)^2$ and $U_k(x) = \cos(\pi k x/l)$. From this ansatz, we obtain that:

$$\left[\omega_k \left(\frac{\mathbb{C}}{1 + \lambda_k l_m^2} + \phi^* \mathbb{I} \right) + \lambda_k \mathbb{K} \left(D \mathbb{I} - \frac{D_m \mathbb{C}}{1 + \lambda_k l_m^2} \right) - \mathbb{J} \right] \underline{X}_i^k = 0$$

where,

$$\mathbb{C} = \begin{pmatrix} \chi_A & \chi_I r^{-1} \\ \chi_A r & \chi_I \end{pmatrix} \text{ with } r = \frac{A_i^*}{I_i^*}.$$

Thus, unstable spatial modes are those for which a ω_k with a positive real part solves the dispersion relation:

$$\det \left[\omega_k \left(\frac{\mathbb{C}}{1 + \lambda_k l_m^2} + \phi^* \mathbb{I} \right) + \lambda_k \mathbb{K} \left(D \mathbb{I} - \frac{D_m \mathbb{C}}{1 + \lambda_k l_m^2} \right) - \mathbb{J} \right] = 0. \quad [12]$$

To be in line with the classical Turing's model, we impose that the homogeneous solution in the absence of spatial terms ($\lambda_k = 0$) is stable. Thus the two solutions ω^0 of

$$\det [\omega^0 (\mathbb{C} + \phi^* \mathbb{I}) - \mathbb{J}] = 0,$$

have negative real parts. Such condition is satisfied as soon as

$$\phi^* + \text{tr } \mathbb{C} > 0, \text{ det } \mathbb{J} > 0 \text{ and } \phi^* \text{tr } \mathbb{J} + \text{det } \mathbb{J} \text{tr } (\mathbb{J}^{-1} \mathbb{C}) < 0. \quad [13]$$

Otherwise, the homogeneous solution can lose stability even without spatial terms and the steady state would then oscillate in time. These conditions generalize the classical ones (39), $\text{det } \mathbb{J} > 0$ and $\text{tr } \mathbb{J} < 0$ obtained for $\chi_{A,I} = 0$.

In the main text (*cf.* Fig. 2A), we study the dispersion relation Eq. (12) in the case where \mathbb{J} is computed based on the classical activator-inhibitor scheme Eq. (8) and $\chi_I = 0$ since conditions Eq. (13) are automatically satisfied in this case. With such choice, the instability of the homogeneous state is a pitchfork bifurcation, meaning that at the onset of instability, the imaginary part of the unstable(s) mode(s) ω_k is zero.

Among the unstable λ_k (i.e. those associated with a positive ω_k), we can select the most unstable one (i.e. the one associated with the largest value of ω_k) in the dispersion relation Eq. (12). This wavelength λ_u is the one which grows with the largest rate and is therefore likely to be the observed one in a numerical simulation of Eq. (10). However, this result should not be considered as rigorous given that there may be other non-linear effects selecting the wavelength which escape this analysis. To complement Fig. 2A of the main text, we show on Fig. S1 a contour plot of the values of λ_u in the $(K_I/K_A, D_m/D)$ phase space. In the Turing limit (captured by $D_m/D \ll 1$ in Fig. 2A of the main text), λ_u depends very weakly on the ratio K_I/K_A given that this ratio has to be large for the instability to occur in the first place. Therefore λ_u is mostly controlled by the turnover rates (fixed in Fig. S1) in this case. In the Keller-Segel limit (captured by $K_I/K_A \ll 1$ on Fig 2(a) of the main text), the most unstable wavelength depends on both the turnover rates (fixed) and the ratio D_m/D which explains its variation along this axis. Note that the number of patterns shown in direct numerical simulations shown in Fig. 2B of the main text satisfy this linear prediction of the total number of patterns because they are close to the onset of instability.

To complement this analysis, we also show that considering non-vanishing χ_I , but remaining within the admissible bounds of Eq. (13), can lead to the existence of a third phase representing a Hopf bifurcation where the solution becomes oscillatory. Although interesting, this goes beyond the scope of our analysis, which concentrates on steady-state spatial patterns, and live-imaging would be needed to verify whether complex time-oscillations can occur during pattern formation in embryogenesis. We illustrate however this dynamic behavior in Fig. S2, in which we also show direct numerical simulations of Eq. (10) to justify this claim. We did not find other type of instabilities than the Turing, Keller-Segel and oscillatory ones regardless of the sign of χ_A and χ_I in the case of a classical activator-inhibitor scheme.

E. Cross-diffusion Turing patterns. Another case of special interest is when the cell volume fraction sensitivities to morphogen levels are negative ($\chi_{A,I} < 0$), eliminating the possibility of up-hill morphogen diffusion at the origin of the Keller-Segel instability in Eq. (12).

To simply explain the physical nature of the instability developing here, we first set $\tau = 0$ (leading to $l_m = 0$) such that the tissue volume fraction always locally remains at its homeostatic value. We also assume that the sensitivities of the volume fraction are small $\chi_{A,I} \ll 1$, but that the effective fickian and hydrodynamic diffusivities $D\mathbb{K} \sim D_m\mathbb{K}\mathbb{C}$ remain finite and of the same order of magnitude. Here the aim is not to quantitatively justify these limits from a biological standpoint, given the lack of quantitative measurements of $\chi_{A,I}$, but our goal is to give a qualitative explanation of the instability in a mathematically tractable setting (although the core mechanism we describe does not depend on this assumption).

In this limit, the conditions for linear stability of the homogeneous system Eq. (13) reduces to the classical ones while the dispersion relation Eq. (12) reads:

$$\det [\omega_k \phi^* \mathbb{I} + \lambda_k \mathbb{K} (D\mathbb{I} - D_m\mathbb{C}) - \mathbb{J}] = 0. \quad [14]$$

Interestingly, this relation of dispersion has been studied for monophasic reaction-diffusion systems with *ad hoc* cross-diffusion terms (40). We also refer to (41) for further exposure of the potential physical origin of cross-diffusion terms in reaction-diffusion systems. As shown in (40), such cross-diffusion terms result in a dramatic broadening of the patterns phase space. In particular, any two-morphogen reaction scheme (inhibitor-inhibitor, activator-activator, etc.) has the potential to generate spatial patterns and not just the classical activator-inhibitor scheme.

F. Generalized Turing instability case. We now get back to the general case of system Eq. (6) but assume that $\chi_{A,I} = 0$ such that cell volume fraction is not sensitive to morphogen concentration. In this case, the last equation uncouples and relaxes to $\phi \equiv \phi^*$ such that Eq. (6) reduces to,

$$\begin{aligned} \phi^* \partial_t \underline{X}_i &= \underline{F}(\underline{X}_i) + \Gamma \underline{X}_e - \Lambda \underline{X}_i \\ (1 - \phi^*) \partial_t \underline{X}_e - D \nabla^2 \underline{X}_e &= -\Gamma \underline{X}_e + \Lambda \underline{X}_i \end{aligned} \quad [15]$$

The linear stability of the homogeneous solution $\underline{X}_i \equiv \underline{X}_i^*$, $\underline{X}_e \equiv \mathbb{K} \underline{X}_i^*$ of Eq. (15) reduces to the dispersion relation

$$\det [(\omega_k(1 - \phi^*) + D\lambda_k) (\omega \phi^* \mathbb{I} - \mathbb{J} + \Lambda) + (\omega \phi \mathbb{I} - \mathbb{J}) \Gamma]. \quad [16]$$

In the main text, we consider the double limit:

$$\Gamma \gg \Lambda \gg \mathbb{J},$$

in which case, the above relation reduces to the classical (39) Turing case,

$$\det [\omega \phi \mathbb{I} + \lambda_k D \mathbb{K} - \mathbb{J}],$$

and the analogue of Eq. (15) reads:

$$\phi^* \partial_t \underline{X}_i - D \mathbb{K} \nabla^2 \underline{X}_i = \underline{F}(\underline{X}_i).$$

While it is clear from a biological standpoint that $\Gamma, \Lambda \approx 10^{-2} \text{ s}^{-1} \gg \mathbb{J} \approx 10^{-4} \text{ s}^{-1}$, (37), it is not clear that $\Gamma \gg \Lambda$. However, we note that the Turing instability typically holds in this limiting case. As a matter of fact, the opposite limit where $\Lambda \gg \Gamma$ does not lead to patterns. Indeed, in the case

$$\Lambda \gg \Gamma \gg \mathbb{J},$$

Eq. (16) reduces to:

$$\det [\omega(1 - \phi^*)\mathbb{1} + \lambda_k D\mathbb{1} - \mathbb{J}\mathbb{K}^{-1}],$$

which cannot lead to a patterning instability in general as it corresponds to a case where the diffusion coefficients for the activator and the inhibitor are the same. This result is interesting as it might have particular biological implications, leading for example to the prediction that cells might generate stable spatial patterns of morphogens mostly in up- or down-regulating their endocytosis machinery in order to modulate the transmembrane transport equilibrium constants and consequently the values of morphogen effective diffusion coefficients.

G. Single morphogen case. We now consider the general case where a single morphogen exists which we chose by convention to be A . In that case, Eq. (6) simplifies to:

$$\begin{aligned} \partial_t(\phi A_i) &= f(A_i) + \gamma_A A_e - \lambda_A A_i \\ \partial_t((1 - \phi)A_e) + \nabla \cdot (A_e D_m \nabla \phi - D \nabla A_e) &= -\gamma_A A_e + \lambda_A A_i \\ \partial_t \phi - \nabla \cdot (D_m \nabla \phi) &= \frac{\phi_h(A_i) - \phi}{\tau}. \end{aligned} \quad [17]$$

where $f(A_i) = (A_i^* - A_i)/\tau_A$ is the linearized form of f .

G.1. Robustness with respect to the main text limit. In the main text, system Eq. (17) is studied in the limit where $\gamma_A \gg \lambda_A \gg 1/\tau_A$ and $\tau/\tau_A \sim K_A \ll 1$ and thus reduces to:

$$\begin{aligned} \partial_t(\phi A_i) + K_A \nabla \cdot (A_i D_m \nabla \phi - D \nabla A_i) &= f(A_i) \\ -l_m^2 \nabla^2 \phi + \phi &= \phi_h(A_i). \end{aligned} \quad [18]$$

However, an explicit criterion for the linear stability of Eq. (17) can be obtained where instead of such complex limit, we simply postulate (only for sake of simplicity) that $\phi^* \simeq 1$. While $\gamma_A, \lambda_A \gg 1/\tau_A$ is verified in biological situations, this is particularly helpful to demonstrate that the instability we find in the single morphogen case does not rely on the assumption $\gamma_A \gg \lambda_A$. The condition for an instability to occur in Eq. (17) (when the characteristic domain size $l \gg \sqrt{D\tau_A}$) reads,

$$\sqrt{\frac{D}{D_m} \left(1 + \frac{1}{K_A \gamma_A \tau_A}\right)} + \sqrt{\frac{\tau}{K_A \tau_A}} < \sqrt{\chi_A}, \quad [19]$$

which can be further reduced to the condition formulated in the main paper:

$$\sqrt{\frac{D}{D_m}} + \sqrt{\frac{\tau}{K_A \tau_A}} < \sqrt{\chi_A}, \quad [20]$$

in the biologically meaningful case (see Section G.3) where $K_A \gamma_A \tau_A \gg 1$. To further demonstrate this claim we present on Fig. S3 direct numerical simulations displaying steady state patterns for large and small values of K_A .

G.2. Scaling properties of Keller-Segel patterns. In this section, we consider only the special case where $\tau_A \rightarrow \infty$ and $K_A \rightarrow 0$ while $K_A D_m, K_A D$ and τD_m remain finite. This limit corresponds to a case where the morphogen turnover rate is very slow but where the effective fickian and hydrodynamic diffusivities remain nonetheless finite. In such case, Eq. (17) reduces to a classical Keller-Segel system (42):

$$\begin{aligned} \partial_t(\phi A_i) + K_A \nabla \cdot (A_i D_m \nabla \phi - D \nabla A_i) &= 0 \\ -l_m^2 \nabla^2 \phi + \phi &= \phi_h(A_i), \end{aligned} \quad [21]$$

but with a slightly different dynamics (ϕA_i instead of A_i in the time derivative) and a non-linear dependence of ϕ on A_i through ϕ_h . A very similar equation was derived and studied in the context of active gels (38, 43).

Integrating the first equation of Eq. (21), steady states of Eq. (21) are given by

$$-l_m^2 \nabla^2 \phi + \phi = \phi_h \left(A_i^* \frac{e^{\frac{D_m}{D} \phi(\vec{r})}}{\langle e^{\frac{D_m}{D} \phi} \rangle} \right), \quad [22]$$

where $\langle h \rangle = |\Omega|^{-1} \int_{\Omega} h(\vec{r}) d\vec{r}$ denotes the spatial average over the tissue domain Ω . For simplicity, we now consider Eq. (22) on the finite segment $[0, l]$ for which $\lambda_k = (\pi k/l)^2$, and investigate the possible bifurcations arising from the homogeneous state when the volume fraction sensitive parameter χ_A increases. Using the continuation software AUTO (44), we numerically compute the first three branches of such bifurcation diagram on Fig. S4 (a). It features an infinite number of critical points $\chi_A^k = D/D_m(1 + l_m^2 \lambda_k)$ from where inhomogeneous solutions bifurcate, see Fig. S4 (c).

Similar to (38, 43), we numerically show that starting from an arbitrary distribution of A_i and if an instability exists, the system Eq. (21) will always coarsen to a single ‘‘two-zones’’ pattern corresponding to the fundamental mode of the instability λ_1 . The reason for this is that morphogen concentration creates a non-local convergent (since χ_A positive) flow recruiting even more morphogens over the hydrodynamic length l_m and further increasing the flow. This positive feedback loop would lead to infinite localization of the morphogen concentration if morphogen diffusion was not preventing such a blow up by penalizing

the creation of sharp gradients in concentration. If χ_A is small, the diffusion dominates and the concentration of morphogen is homogeneous but when χ_A reaches the critical threshold χ_A^1 , the morphogen self-organize into a fundamental pattern where active advective transport balances diffusion. This is known as the Keller-Segel instability. Because the positive feedback loop is non-local, the morphogens concentration always coarse-grains into the fundamental mode. Interestingly, we found using a classical normal mode analysis, and confirmed numerically, that the nature of this first bifurcation branch is of pitchfork type but can be supercritical (second order phase transition) or subcritical (first order phase transition) *cf.* Fig. S4 (b). In practice, this means that two steady states corresponding to a non-patterned and a patterned state may co-exist for a range of parameters in the subcritical case. The transition from one state to the other could be then controlled by additional regulatory pathways.

Next, we define the fundamental pattern size as $l_{\text{pat}} = \int_0^l H(A_i(x) - A_i^*) dx$, where the Heaviside function selects the part of the morphogen profile larger than its average value. Therefore $l_{\text{pat}} = 0$ for the homogeneous solution and becomes non-zero when a pattern forms. We show on Fig. S5 that this pattern scales as a function of the domain size for various values of χ_A . These results demonstrate that when an instability exists, a single “two zones” pattern always forms and its size scales with an increase in tissue domain size. This scaling property is at odds with what is observed for a classical Turing instability, where additional patterns form as the domain size increases. Thus, in this limit, our model constitutes a suitable theory to explain the scaling properties of various “two-zones” developmental patterns such as the dorso-ventral pattern of *Xenopus* (45), the antero-posterior pattern of planarian (46) or the left-right pattern of zebrafish (47).

G.3. Biological relevance of the Keller-Segel instability. Here, we briefly review the orders of magnitude from the main text, to justify in particular that the Keller-Segel-Turing phase diagram proposed in Fig. 2A of the main text is relevant given the reported orders of magnitude for the model parameters. We focus here on the Keller-Segel instability and Eq. (19). The hypothesis $K_A \gamma_A \tau_A \gg 1$ is rather straightforward to fulfil, as typical values measured in the literature are $\tau_A \approx 10^4 - 10^5$ s (47), while $\gamma_A \approx 10^{-1} - 10^{-2} \text{ s}^{-1}$ (37). Therefore, even for small values of K_A , the approximation is expected to hold (as values at which it would break down, $K_A < 10^{-3}$, would imply that almost no morphogen is present in the extracellular space anymore). This shows that the instability condition derived in the main paper for the Keller-Segel instability is in fact robust with respect to the assumption that $K_A \ll 1$, as opposed to the Turing instability with re-normalized diffusion coefficients which require $K_A \ll 1$.

Thus, one can adopt the simplified instability criteria Eq. (20), where $\sqrt{\frac{D}{D_m}}$, $\sqrt{\frac{\tau}{K_A \tau_A}}$ and $\sqrt{\chi_A}$ must be compared. Because χ_A is the least experimentally known of the model parameters, we start by focusing on the first two quantities. Orders of magnitude from the main text allow us to estimate $\tau/(K_A \tau_A) \approx 0.01 - 0.1$. Moreover, D_m can adopt a wide range of values given the wide range of length scales of extracellular gaps in different tissues, but its value is consistently larger to much larger than D , with $D/D_m \approx 10^{-4} - 1$, which tends to say that that $\tau/(K_A \tau_A)$ is the main factor resisting the Keller-Segel instability in the limit of large hydrodynamic diffusion D_m (*i.e.* when the intercellular spaces are $\approx 0.1 \mu\text{m}$). In this case, the cell volume sensitivity to morphogen concentration, χ_A , must be larger than $0.01 - 0.1$ for the Keller-Segel instability to develop, which, although relatively little data exists on variations of ϕ in embryonic tissues, is a rather lax criterion, as it represents typical variations of ϕ of only $1 - 10\%$ with morphogen concentration. One should note that for very compact tissues, where values of $\sqrt{D/D_m}$ could be close to unity, the instability could require unrealistically large values of χ_A and thus would be screened.

H. Linking FRAP and FCS measurements of the diffusion coefficient. Fluorescence recovery after photobleaching (FRAP) is a method which has been long used to experimentally determine diffusion coefficients (48). More particularly, it has been employed recently in several *in vivo* systems such as the early Zebrafish (47) and *Xenopus* (45) embryos or the *Drosophila* wing disk (49) in order to measure tissue-wide effective diffusion coefficients of various morphogens. Nevertheless, establishing a correspondence between these FRAP measured diffusion coefficients and the effective diffusion coefficient defined in our modeling framework requires some care.

Indeed, in such FRAP experiments, the endogeneous molecule of interest is usually replaced by a genetically engineered copy which has been fused to a fluorescent protein such as the GFP. Thus, if one wants to study simultaneously two interacting morphogens, one needs to genetically engineer two constructs with two different fluorescent protein tags. In practice this is rarely the case and the diffusive properties of each morphogen are studied independently (45, 47). Moreover, such an approach does not directly discriminate the internal and external fractions of a given morphogen. Therefore, the intensities of fluorescence are proportional to the total concentration of a given morphogen : $A_t = \phi A_i + (1 - \phi) A_e$ for A and $I_t = \phi I_i + (1 - \phi) I_e$ for I . Combining the conservation equations Eq. (2) and Eq. (3), we obtain:

$$\begin{aligned} \partial_t A_t + \nabla \cdot (A_e D_m \nabla \phi - D \nabla A_e) &= f(A_i, I_i) \\ \partial_t I_t + \nabla \cdot (I_e D_m \nabla \phi - D \nabla I_e) &= g(A_i, I_i) \\ \partial_t \phi - \nabla \cdot (D_m \nabla \phi) &= \frac{\phi_h(A_i, I_i) - \phi}{\tau}. \end{aligned} \quad [23]$$

For a small enough bleached region, the contribution of morphogen turnover rates can be neglected and the fluorescence recovery is mostly driven by transport, as shown in the case of the Zebrafish embryo (47). For the sake of simplicity, we shall thus proceed under this assumption, although some other *in vivo* systems may require to account for morphogen turnover rates (50).

The classical Turing case corresponds to a fixed volume fraction $\phi = \phi^*$ implying $v_e = 0$. As equations for A and I uncouple, we can focus on a single morphogen only (say A) and the fluorescence A_t satisfies:

$$\begin{aligned} \partial_t A_t - \nabla \cdot (D \nabla A_t) &= 0 \\ \phi^* \partial_t A_t &= \gamma_A A_t - \lambda_A A_t \\ A_t &= \phi^* A_i + (1 - \phi^*) A_e. \end{aligned} \quad [24]$$

From Eq. (24), we can deduce the following dispersion relation:

$$(1 - \phi^*) \omega^2 + \left(\gamma_A + \lambda_A \frac{1 - \phi^*}{\phi^*} + D \lambda_k \right) \omega + \frac{\lambda_A D \lambda_k}{\phi^*} = 0,$$

where λ_k are the eigenvalues of the Laplace operator over the bleached region of typical size L_b and ω the rates associated with fluorescence recovery. Non dimensionalizing times with γ_A^{-1} and introducing the non-dimensional quantity $\Delta = D/(\gamma_A L_b^2)$ we can rewrite the above equation as:

$$(1 - \phi^*) \bar{\omega}^2 + \left(1 + K_A \frac{1 - \phi^*}{\phi^*} + \rho_k \Delta \right) \bar{\omega} + \frac{K_A \rho_k \Delta}{\phi^*} = 0, \quad [25]$$

where $\bar{\omega}$ are non-dimensional rates and $\rho_k = L_b^2 \lambda_k$ is a positive non-dimensional geometric factor which increases quadratically with the order of the eigenvalue considered. For instance if the bleached region is spherical, ρ_k is the discrete set of zeros of the Bessel functions of the first kind (48). If the bleached region is $\sim 100 \mu\text{m}$ (47), we have that $L_b^2 \gamma_A \sim 10^{-9} \text{m}^2 \text{s}^{-1}$ suggesting that $\Delta \ll 1$ in Eq. (25). Then at first order we have

$$\bar{\omega}_1 = -\frac{K_A(1 - \phi^*) + \phi^*}{\phi^*(1 - \phi^*)} \quad \text{and} \quad \bar{\omega}_2 = -\frac{K_A \rho_k \Delta}{K_A(1 - \phi^*) + \phi^*},$$

where $\bar{\omega}_1 \gg \bar{\omega}_2$ is an homogeneous clearance rate of fluorescence that is important only at very short timescales while $\bar{\omega}_2$ corresponds to the measured diffusion driven recovery with effective diffusion coefficient,

$$D_{\text{FRAP}} = \frac{K_A D}{K_A(1 - \phi^*) + \phi^*}.$$

To relate the effective diffusion coefficient D_{FRAP} to the local diffusion coefficient D_{Fick} measured by Fluorescence Correlation Spectroscopy (FCS), one should recall that D is already a homogenized over a RVE and as such, depends on the tissue packing fraction. A classical way to relate D and ϕ^* is through the Maxwell formula (51):

$$D \simeq D_{\text{Fick}} \frac{1 - \phi^*}{1 + \phi^*/2}.$$

Maxwell's result formally only holds in the dilute approximation where ϕ^* is close to zero but in fact corresponds to the Hashin-Shtrikman (52) upper-bound which is known to hold outside the dilute limit:

$$D \leq D_{\text{Fick}} \frac{1 - \phi^*}{1 + \phi^*/2}.$$

Such bound can be computed irrespective of the microscopic details of tissue geometry meaning that the actual effect of tortuosity is in reality even more pronounced. One can then directly compare the diffusion coefficient measured by FRAP and the one measured by FCS. For instance, in our first case where $\Delta \ll 1$, we obtain:

$$\frac{D_{\text{FRAP}}}{D_{\text{Fick}}} \leq \frac{K_A(1 - \phi^*)}{(\phi^* + K_A(1 - \phi^*))(1 + \phi^*/2)}.$$

Interestingly, Lefty diffusion coefficient in the zebrafish embryo varies only by a factor 2 between FCS and FRAP measurements (47), $D_{\text{FRAP}}/D_{\text{Fick}} \simeq 0.5$. This can hold in the limit of $K_{\text{Lefty}} \gg 1$, since in this case we obtain $D_{\text{FRAP}} \leq \frac{D_{\text{Fick}}}{1 + \phi^*/2}$, which is consistent with the statement of Muller et al. in (47) that there is ‘‘an approximately two- to three-fold decrease in diffusivity in the presence of cells compared to unhindered diffusion in aqueous solution’’. Note that this last bound ($K_{\text{Lefty}} \gg 1$ limit) also corresponds to the one expected for a passive extracellular molecule which does not chemically interact with cells such as an injected dye or a secreted recombinant fluorescent protein (see (50) for experiments of this kind in early Zebrafish embryos). However, if $K_{\text{Lefty}} \lesssim 1$ (concentrations outside of the same order of magnitude or smaller than concentration inside or immobilized), given the large cell volume fraction inferred in this system ($\phi^* \approx 0.8 - 0.9$)(47), we expect the decrease in effective diffusion due to tortuosity to become much larger: $D_{\text{FRAP}}/D_{\text{Fick}} \leq 0.1$. This argues for the need for precise measurements of K_{Lefty} concomitant to ϕ . Another possibility is to consider the possibility of active contributions to morphogen transport ($v_e \neq 0$ in Eq. (23)) since hydrodynamical diffusion would then, to leading order, rescale passive diffusion in an arbitrary manner as we show below.

If ϕ is no longer assumed to be homogeneous, variations of ϕ may contribute to the fluorescence recovery of the bleached region and one needs to fit the intensities A_t and I_t in Eq. (23) (with $f = g = 0$). A quantitative re-interpretation of the

measurements of (50) in this context requires the spatial knowledge of ϕ and is thus left to future work. As a proof of principle, a simple case can be investigated where $\chi_I = 0$ and $\tau \rightarrow 0$. In this situation Eq. (24) becomes

$$\begin{aligned} \partial_t A_t + \nabla \cdot (A_e D_m \nabla \phi - D \nabla A_e) &= 0 \\ \partial_t(\phi A_i) &= \gamma_A A_e - \lambda_A A_i \\ A_t &= \phi A_i + (1 - \phi) A_e \\ \phi - \phi^* &= \chi_A \frac{A_i - A_i^*}{A_i^*} \end{aligned} \quad \text{which at linear order reads,} \quad \begin{aligned} \partial_t A_t + \nabla \cdot (K_A \chi_A D_m \nabla A_i - D \nabla A_e) &= 0 \\ (\chi_A + \phi^*) \partial_t A_i &= \gamma_A (A_e - K_A A_i) \\ A_t &= (\phi^* + \chi(1 - K_A)) A_i + (1 - \phi^*) A_e. \end{aligned} \quad [26]$$

The generalized dispersion relation then reads,

$$(1 - \phi^*)(\chi_A + \phi^*)\omega^2 + [(\chi_A + \phi^*)(\gamma_A + D\lambda_k) + \lambda_A(1 - \phi^* - \chi_A)]\omega + \lambda_A \lambda_k (D - D_m \chi_A) = 0$$

Next, assuming $\chi_A \ll 1$ while $\chi_A D_m \sim D$ are of the same order of magnitude, we can generalize the previous result obtained for $\chi_A = 0$ to

$$D_{\text{FRAP}} = \frac{K_A(D - \chi_A D_m)}{K_A(1 - \phi^*) + \phi^*}.$$

This shows that the active hydrodynamic transport could contribute to rationalize the diffusion coefficients measured by FRAP. In particular, the inequality between D_{FRAP} and D_{Fick} becomes

$$D_{\text{FRAP}} \leq \frac{K_A(D_{\text{Fick}} - \chi_A K l_i^2 / \eta)(1 - \phi^*)}{(K_A(1 - \phi^*) + \phi^*)(1 + \phi^*/2)},$$

which could explain, among other possibilities of active morphogens transport (53), why in some cases even with $\phi^* \simeq 0.85$ and $K_A \lesssim 1$, D_{FRAP} is only slightly smaller than D_{Fick} .

I. Generalisation of the model in presence of tissue rearrangements. In model Eq. (6), we have systematically assumed that changes of the tissue topology are much slower than the fluid circulation ($v_s \simeq 0$) based on the estimates presented in Section A.3. However, these estimates may substantially vary depending on the biological system and cellular flows have been shown to take place at timescales comparable to fluid flows for various morphogenetic processes (54). We therefore present below an extension of the theory accounting for such flows.

A first consequence of a non-negligible v_s was already discussed in Section A.6 as Eq. (3) now contains a transport term

$$\begin{aligned} \partial_t(\phi A_i) + \nabla(\phi A_i v_s) &= f(A_i, I_i) + \gamma_A A_e - \lambda_A A_i \\ \partial_t(\phi I_i) + \nabla(\phi I_i v_s) &= g(A_i, I_i) + \gamma_I I_e - \lambda_I I_i. \end{aligned} \quad [27]$$

The next step is to obtain the expression of v_e as it enters in Eq. (1) and Eq. (2). For this, we have to generalize the mechanical framework presented in Section A.7 to obtain the analogue of Eq. (5) when the tissue can rearrange. We can do so by introducing a new variable \mathbb{E}_s accounting for the non elastic strain present in the tissue due to the cells rearrangements (55). Thus, this strain is connected to the cell flow through the kinetic relation:

$$\frac{d\mathbb{E}_s}{dt} = \partial_t \mathbb{E}_s + v_s \cdot \nabla \mathbb{E}_s = \nabla v_s. \quad [28]$$

In this case, the constitutive behavior Eq. (4) becomes

$$\begin{aligned} \sigma &= 2G(\mathbb{E} - \mathbb{E}_s) + \left(K - \frac{2G}{3}\right) \text{tr}(\mathbb{E} - \mathbb{E}_s) \mathbb{1} - \alpha p \mathbb{1} \\ p &= -\frac{K_u - K}{\alpha} \text{tr}(\mathbb{E} - \mathbb{E}_s) - \frac{K_u - K}{\alpha^2} \delta \phi - (1 - \phi^*) \frac{K_u - K}{\alpha^2} \text{tr}(\mathbb{E}_s). \end{aligned} \quad [29]$$

If we continue to assume that the interstitial fluid flow in the tissue is described by Darcy's law and that the physiologically relevant limit $K_u \gg K \gg G$ and $\alpha \simeq 1$ still holds, we obtain using force balance that:

$$(1 - \phi)(v_e - v_s) = -\frac{\kappa}{\eta} \nabla p = \frac{K\kappa}{\eta} (\nabla \phi + (1 - \phi^*) \nabla \text{tr}(\mathbb{E}_s)).$$

Eliminating v_e and denoting $\epsilon_s = \text{tr}(\mathbb{E}_s)$ we can rewrite the full model as

$$\begin{aligned} \partial_t(\phi \underline{X}_i) + \nabla \cdot (\phi \underline{X}_i v_s) &= \underline{F}(\underline{X}_i) + \mathbb{T} \underline{X}_e - \mathbb{A} \underline{X}_i \\ &\quad \partial_t((1 - \phi) \underline{X}_e) + \\ \nabla \cdot ((1 - \phi) \underline{X}_e v_s + D_m(\nabla \phi + (1 - \phi^*) \nabla \epsilon_s) \underline{X}_e - D \nabla \underline{X}_e) &= -\mathbb{T} \underline{X}_e + \mathbb{A} \underline{X}_i \\ \partial_t \phi - \nabla \cdot ((1 - \phi) v_s + D_m(\nabla \phi + (1 - \phi^*) \nabla \epsilon_s)) &= \frac{\phi h(\underline{X}_i) - \phi}{\tau} \\ \partial_t \epsilon_s + v_s \cdot \nabla \epsilon_s &= \nabla \cdot v_s. \end{aligned} \quad [30]$$

Such model generalizes Eq. (6) in the presence of a given cellular flow v_s . Large scale cellular flows are ubiquitous during developmental morphogenesis (56) but their genesis is far from being understood and a general assessment of their influence on our system is not presently within reach. Thus, for the sake of clarity and to extract the key biophysical ingredients generating the instabilities described in the main text, we have decided to work in the limit where $v_s = 0$.

However, we first note that if the cell flow is not associated with volumetric changes in the tissue (i.e. $\nabla \cdot v_s = 0$) as it has been verified for example during the ventral furrow formation of *Drosophila* (57) or in limb bud morphogenesis (58), then $\epsilon_s = 0$. In this case, the homogeneous solution Eq. (7) is still a solution of Eq. (30) which can be rewritten,

$$\begin{aligned} \frac{d\phi X_i}{dt} &= F(X_i) + \mathbb{F}X_e - \mathbb{A}X_i \\ \frac{d(1-\phi)X_e}{dt} + \nabla \cdot (D_m \nabla \phi X_e - D \nabla X_e) &= -\mathbb{F}X_e + \mathbb{A}X_i \\ \frac{d\phi}{dt} - \nabla \cdot (D_m \nabla \phi) &= \frac{\phi_h(X_i) - \phi}{\tau}. \end{aligned} \quad [31]$$

where $d/dt = \partial_t + v_s \cdot \nabla$ is the material derivative with respect to the cellular flow. As such, the only effect of the cellular flow is to add a transport term to Eq. (6). The impact of v_s on the stability properties of Eq. (6) presented in the main paper can then be investigated case by case either by modeling v_s or by at least checking its order of magnitude. For example for the limb bud morphogenesis $v_s \approx 0.01 \mu\text{m/s}$ (58, 59), while from our estimates the typical velocity of the interstitial flow driven by spatial changes in the porosity $\sqrt{D_m/\tau} \approx 0.1 - 10 \mu\text{m/s} \gg v_s$. We therefore do not expect that cell rearrangements will substantially modify the thresholds of patterning instabilities given in the main text, as they are happening at a slower rate than our morphogen-driven pattern formation mechanism. A word of caution for this specific system though, as we note that our model requires the existence of at least a transient elastic tissue structure *i.e.* the existence of some transient level of physical connections between the cells, either directly via some adhesion or indirectly via the Extracellular Matrix (ECM). Such an hypothesis and the measurements of the ensuing elastic moduli would need to be carefully scrutinized for validating the application of our model to this specific example.

A second simple modeling assumption that can be used to generalize our results is to suppose that morphogens are driving the cellular flow according to

$$v_s = \underline{\vartheta} \cdot \nabla X_e \quad [32]$$

where $\underline{\vartheta} = (\vartheta_A, \vartheta_I)$ is a vector of chemotactic sensitivities of the cell motion with respect to the morphogens concentrations. Such a chemotactic role of morphogens has been demonstrated in particular examples such as Shh in *Drosophila* (60). In this case, Eq. (30) is a closed system of equations which stability can be investigated. Clearly, all the instabilities presented in the paper will remain valid for small enough $\underline{\vartheta}$. In the more general case, new instabilities associated with chemotaxis will appear. In particular, we can illustrate this in the simple case where only one morphogen is present as in Section G.1 and in the limit considered in the main paper where $\gamma_A \gg \lambda_A \gg 1/\tau_A$ and $\tau/\tau_A \sim K_A \ll 1$. If that case, if $\chi_A = 0$, we have shown that no instability occurs in Eq. (18) as Eq. (20) is not satisfied. This is no longer true if we consider that $\vartheta_A > 0$ as we find the onset of an oscillatory (Hopf) instability when:

$$\frac{(2\phi^* - 1)\vartheta_A A^*}{D_m} < \frac{D}{D_m} < \frac{\tau}{K_A \tau_A} + \frac{\vartheta_A A^* \phi^*}{D_m} - 2\sqrt{\frac{(1 - \phi^*)\vartheta_A A^* \tau}{D_m K_A \tau_A}}.$$

While the first inequality ensures that chemotaxis is not too strong, such that it would make an infinite number of high modes unstable by surpassing Fickian diffusion, the second inequality shows that chemotaxis alone can be enough to destabilize the regularizing effects of both Fickian and hydrodynamic diffusion as well as the morphogen chemical turnover. In general, that type of instability will combine with the ones presented in the main text but a systematic investigation of such cross-effects is left to future works.

2. Historical background

In 1948, Turing's long time interest for biology took a new twist, largely influenced by the works of D'Arcy Thompson and Conrad Waddington (61). In this context, he decided to study pattern formation and morphogenesis during embryonic development, developing computer programs to numerically solve the complex partial differential equations resulting of his abstraction of the biological question. In a letter dated of 12 February 1951, he wrote to a former colleague and friend, Mike Woodger (62):

“Our new machine is to start arriving on Monday. I am hoping as one of the first jobs to do something about ‘chemical embryology’“

These “jobs” would be the foundations of Turing's famous paper “The Chemical Basis of Morphogenesis” (63). In this article, he proposed an elegant mathematical model of self-organisation, where two reacting chemicals can spontaneously form periodic spatial patterns through an instability driven by their difference in diffusivity. This idea was not only very influential amongst biologists such as J.M. Smith (64) and L. Wolpert (65), or physicists such as I. Prigogine (66), F. Crick (67) and H. Meinhardt (35), but was at the stem of a new class of PDE models which became central in the development of modern mathematical biology (39, 68). However, given the lack of molecular and cellular evidences available at that time, in a lot of studies, the emphasis was often placed on the striking similarity of the patterns obtained by the model with those observed in biological systems such as animal coat and skin pigmentation patterns, rather than on discussing the biological validity of the modeling assumptions. Quite astonishingly, in a letter to Alan Turing dated of 11 September 1952, Waddington already raised similar concerns about the applicability of Turing's reaction-diffusion model to biological developmental systems, questioning its limitation to reproduce some observed behaviours in embryonic development such as pattern scaling with tissue size or the generation of a spatial pattern of discrete cell types (69):

“I was extremely interested to read your recent paper on the chemical basis of morphogenesis. [...] I rather doubt, however, whether the kind of processes with which you were concerned play a very role in the fundamental morphogenesis which occurs in early stages of development. [...] Even in a case like the regeneration of tentacles in Hydra the final result seems to me more regular than one would expect from your type of mechanism. For instance, if one splits two hydras longitudinally and places them together so that the split edges heal and forms a single tube of double the normal diameter, this enlarged tube still regenerates the normal number of tentacles, although it would, of course, contain twice the normal ‘chemical wave-lengths’ around its circumference.”

Turing was not naive about the limitations and underlying assumptions of his model and in fact already hints, in his article, at possible extensions to his theory considering the structure and mechanical properties of biological tissues (63):

“[...] one proceeds as with a physical theory and defines an entity called ‘the state of the system’[...] The description of the state consists of two parts, the mechanical and the chemical [...] In determining the changes of state one should take into account: (i) The changes of position and velocity as given by Newton’s laws of motion. (ii) The stresses as given by the elasticities and motions, also taking into account the osmotic pressures as given from the chemical data (iii) The chemical reactions (iv) The diffusion of the chemical substances. The region in which this diffusion is possible is given from the mechanical data. [...] The interdependence of the chemical and mechanical data adds enormously to the difficulty, and attention will therefore be confined, so far as is possible, to cases where these can be separated.”

The original work of Hans Othmer on the transition between discrete and continuous models of pattern formation in tissues in the 1970’s (70) is maybe the closest example of this new research program tangentially set by Turing in his paper. In introduction of a review article entitled “Current problems in pattern formation” Othmer wrote (71):

“In Turing’s work and virtually all subsequent work, the only mode of transport considered is diffusion. Furthermore, the model systems all deal with structureless, tightly coupled cells or their continuum analogs. Some future work should be directed toward: (a) the analysis of other modes of transport (b) more realistic models of cell and tissue structure and, (c) networks of cells that communicate only indirectly via the external medium.”

As early attempts to fulfil this program, we would like to highlight the work of L.E. Scriven, who used the coupling of mechanical forces with chemical reactions to describe spontaneous fluid transport(72), paving the way to modern theories of active gels, and the pioneering work of G.F. Oster, one of the fathers of mechanobiology, on limb growth and patterning (73).

A. Methods. Linear stability analysis is performed numerically using conventional algebra packages in Mathematica. Numerical integration of models Eq. (10), Eq. (17) and Eq. (21) are performed in 1D with a custom made code written in Matlab and available on request to the authors. In brief, the code uses a mass conserving finite volume stencil in space and a first order implicit scheme in time.

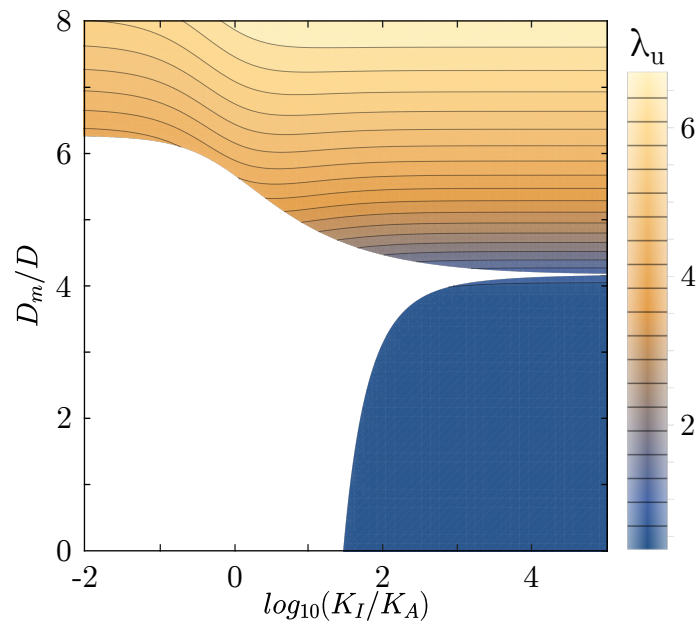


Fig. S1. Estimation of the pattern wavelength using linear stability analysis. Contour plot of the most unstable wavelength obtained using the dispersion relation Eq. (10) in the $(K_I/K_A, D_m/D)$ parameter space shown on Fig. 2 (a) of the main text. parameters are set to $\tau/(K_A\tau_A) = 0.01$, $\chi_A = 0.25$, $\chi_I = 0$, $\tau_I/(K_A\tau_A) = 0.2$, $K_A\tau_A\rho = 1$, $\phi^* = 0.85$ and large tissue size ($l_A/l \ll 1$).

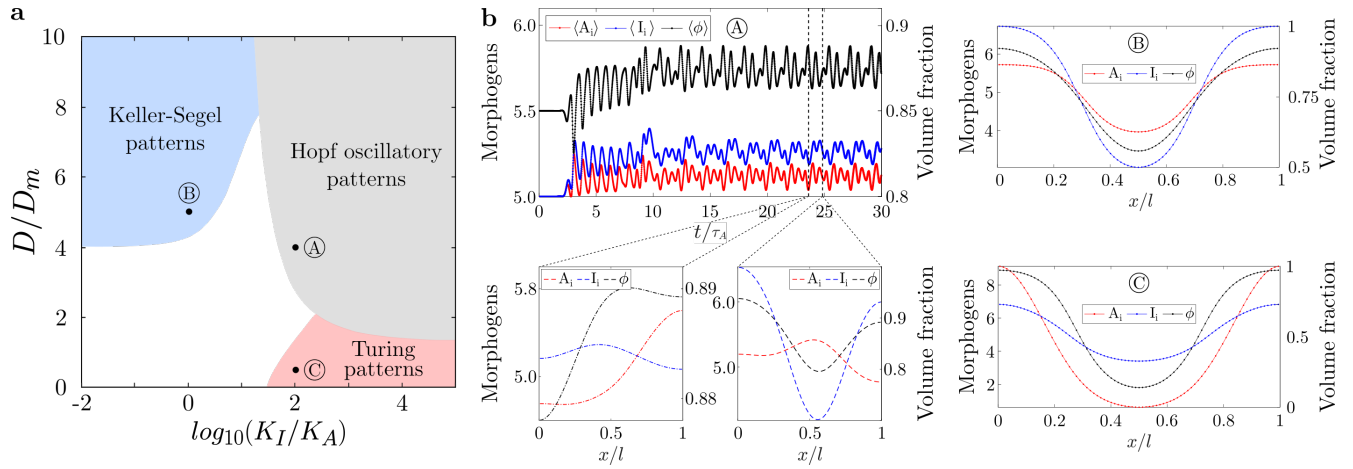


Fig. S2. Patterning instabilities of the simplified model. (a) Phase diagram of Eq. (10) in the $(D_m/D, K_I/K_A)$ parameter space. In blue and red, domains corresponding to pitchfork (first and second order) bifurcations found for Eq. (10) and being respectively Keller-Segel and Turing instabilities. In grey, domain corresponding to a Hopf bifurcation and as such associated with an oscillatory instability. Model parameters are set to $\chi_A = 0.25$, $\chi_I = 1$, $\tau/(K_A\tau_A) = 1$, $\tau_I/(K_A\tau_A) = 0.2$, $K_A\tau_A\rho = 1$, $\phi^* = 0.85$ and $l_A/l \ll 1$. (b) 1D numerical simulations of Eq. (10) for points A, B and C, in the $(D_m/D, K_I/K_A)$ space, as shown in (a). For point A, in the Hopf oscillatory patterns region, spatially averaged morphogens concentrations and volume fraction (denoted with $\langle \cdot \rangle$) do not converge to a constant value but oscillate in time. These temporal oscillations are associated with a periodic oscillation of morphogens and volume fraction spatial profiles. Initial conditions are taken at random and $l_A/l = 0.1$.

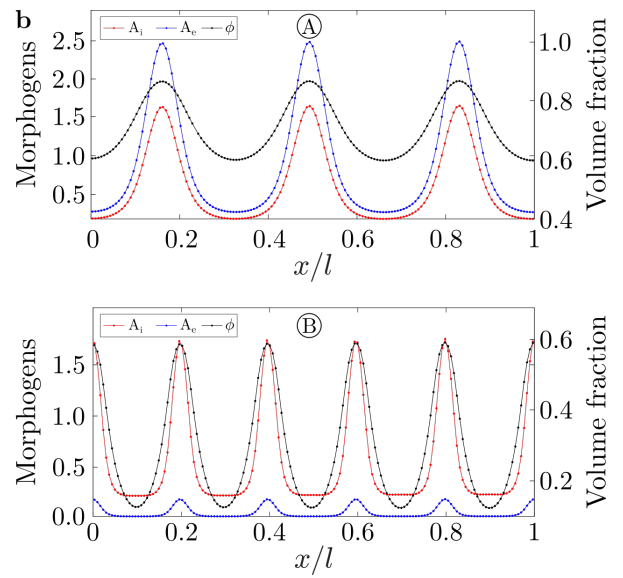
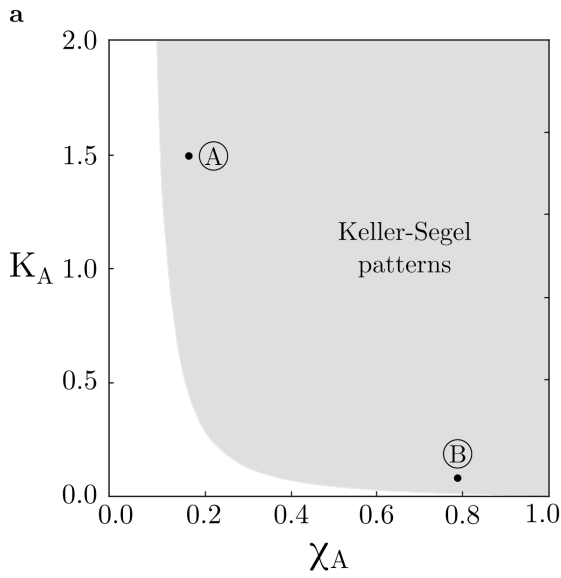


Fig. S3. Keller-Segel instability of the simplified model with one morphogen. (a) Phase diagram of Eq. (17) in the (K_A, χ_A) space is given by Eq. (19). The grey domain correspond to the occurrence of a pitchfork bifurcation in Eq. (17) for $l/\sqrt{D\tau_A} \ll 1$. Other parameters are set to $\gamma_A\tau_A = 0.01$, $\tau/\tau_A = 1$ and $D_m/D = 10$. (b) 1D numerical simulations of Eq. (17) for two points, A and B, in the (K_A, χ_A) space, as shown in (a), corresponding respectively to a large and small value of K_A . Morphogen turnover function is given by the following non-linear form: $f(A_i) = A_i(A_i^* - A_i)/(A_i^*\tau_A)$. Initial conditions are taken at random and $\phi^* = 0.85$, $l_A/l = 0.1$.

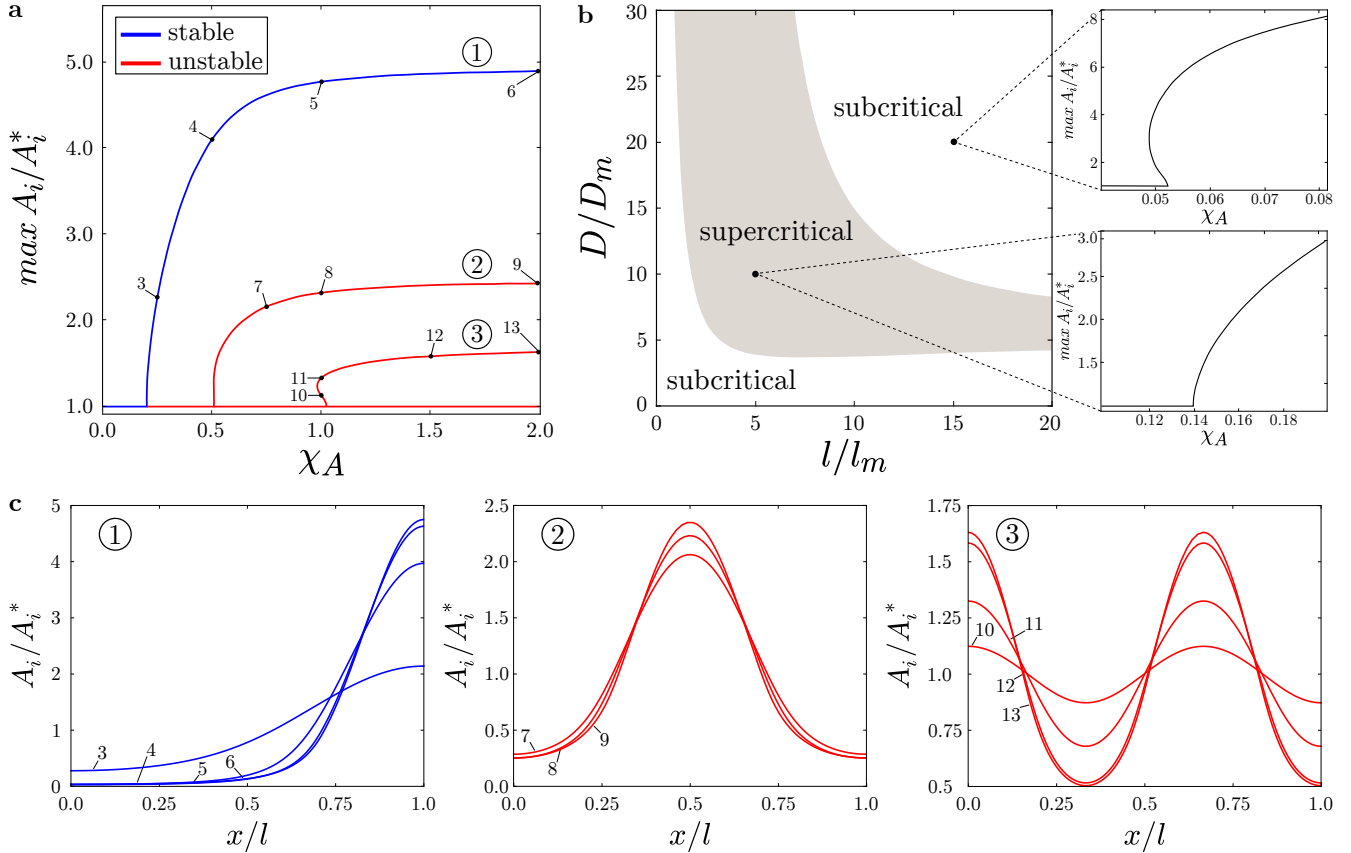


Fig. S4. Bifurcation diagram of the solution Eq. (22) of the simplified model with one morphogen. (a) First branches bifurcating from the homogeneous solution at the onset of instability. Black lines are stable, while red lines are unstable. Stability is obtained numerically in integrating the time dependent problem Eq. (21), starting from the considered steady state solution with a small perturbation. Parameters are $\phi^* = 0.85$, $D_m/D = 10$ and $l/l_m = 3.1$. **(b)** Nature of the fundamental (i.e. first) bifurcation point. Parameter $\phi^* = 0.85$. **(c)** Profiles of activator concentrations along the branches shown in (a) (cf. corresponding labels). Half of a wavelength is added each time the index of the branch is increased by one. Increase in χ_A results in sharper profiles. Only profiles along one branch of the pitchfork bifurcation are shown. The other branch, superimposed on the one shown, corresponds to symmetric profiles in respect with the centre of the space domain.

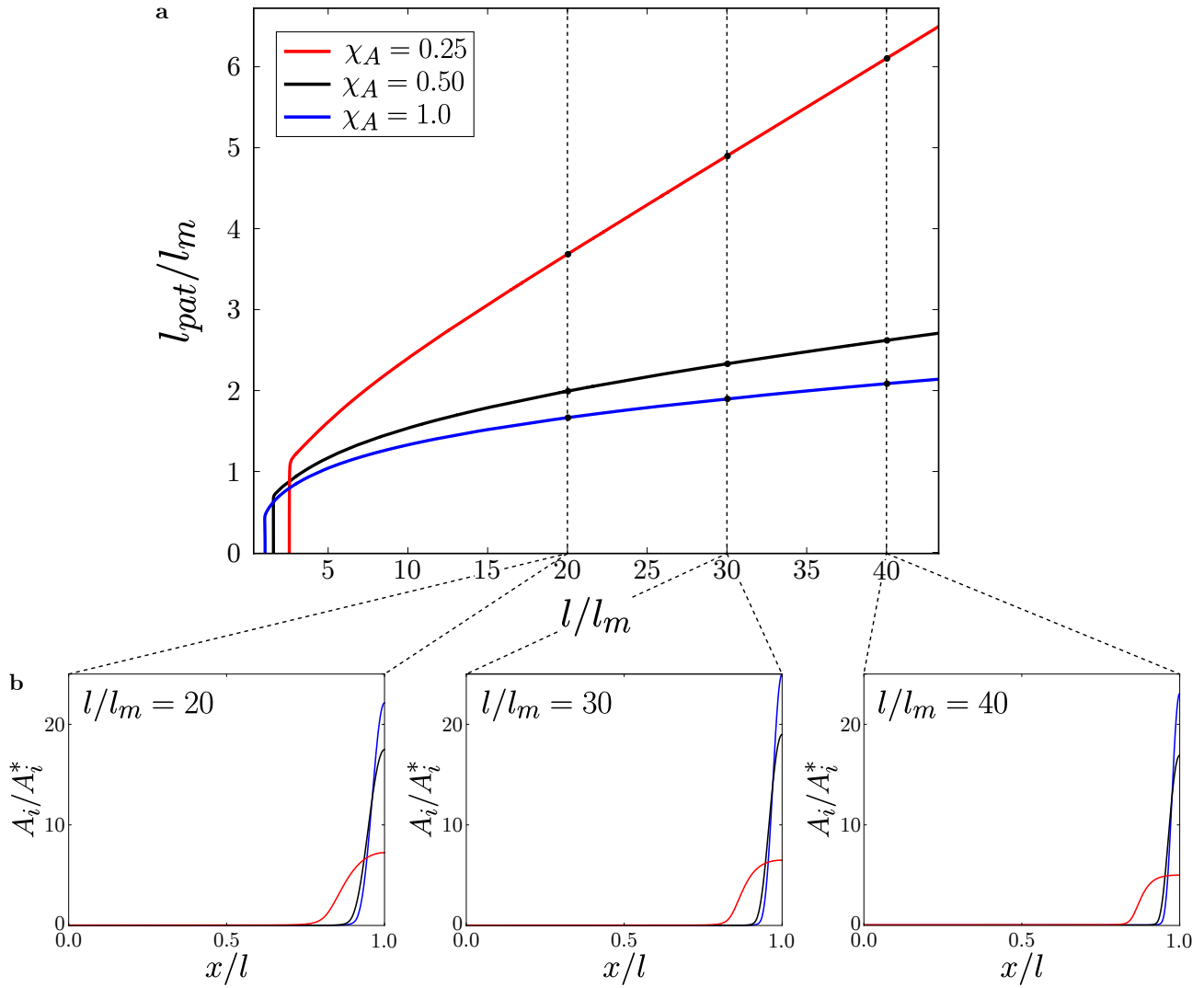


Fig. S5. Scaling of pattern size with domain size, for the simplified model with one morphogen. (a) Size of the pattern as a function of tissue domain size. After the onset of instability, the stable pattern size increases linearly with the domain size for various values of χ_A . Parameters are $D_m/D = 10$ and $\phi^* = 0.85$. (b) Morphogen (activator) concentration profiles along selected point of the branches shown in panel (a).

References

1. Kozlov SM (1979) Averaging of random operators. *Matematicheskii Sbornik (N.S.)* **109**(2):188–202.
2. Bear J, *Dynamics of Fluids in Porous Media* (Dover, New-York, 1989), new edition.
3. Charras GT, Yarrow JC, Horton MA, Mahadevan L and Mitchison TJ (2005) Non-equilibration of hydrostatic pressure in blebbing cells. *Nature* **435**:365.
4. Moeendarbary E *et al.* (2013) The cytoplasm of living cells behaves as a poroelastic material. *Nature Materials* **12**:253.
5. Dolega ME, Delarue M, Ingremeau F, Prost J, Delon A and Cappello G (2017) Cell-like pressure sensors reveal increase of mechanical stress towards the core of multicellular spheroids under compression. *Nature Communications* **8**:14056.
6. Hoffmann EK, Lambert IH and Pedersen SF (2009) Physiology of cell volume regulation in vertebrates. *Physiological Reviews* **89**(1):193-277.
7. Nielsen MS *et al.* (2012) Gap junctions. *Comprehensive Physiology* **2**:1981.
8. Fujimoto K *et al.* (1997) Dynamics of connexins, E-cadherin and alpha-catenin on cell membranes during gap junction formation. *Journal of Cell Science* **110**:311.
9. Szoboszlai M *et al.* (2016) Functional properties of dendritic gap junctions in cerebellar golgi cells. *Neuron* **90**:1043.
10. Nitsche JM, Chang H-C, Weber PA and Nicholson BJ (2004) A transient diffusion model yields unitary gap junctional permeabilities from images of cell-to-cell fluorescent dye transfer between *Xenopus* oocytes. *Biophysical Journal* **86**:2058.
11. Weber PA, Chang HC, Nitsche JM and Nicholson BJ (2004) The permeability of gap junction channels to probes of different size is dependent on connexin composition and permeant-pore affinities. *Biophysical Journal* **87**:958.
12. Pitts JD and Finbow ME (1986) Is the gap junction channel-the connexon-made of connexin or ductin? *Journal of Cell Science (Suppl. 4)*: 239.
13. Batchelor GK, *An Introduction to Fluid Dynamics* (Cambridge University Press, Cambridge, 2000), new edition.
14. Zehnder SM, Suaris M, Bellaire MM and Angelini TE (2015) Cell volume fluctuations in MDCK monolayers. *Biophysical Journal* **108**: 247.
15. Zehnder SM *et al.* (2015) Multicellular density fluctuations in epithelial monolayers. *Physical Review E* **92**:032729.
16. Guevorkian K, Colbert M-J, Durth M, Dufour S and Brochard-Wyart F (2010) Aspiration of biological viscoelastic drops. *Physical Review Letters* **104**:218101.
17. Forgacs G, Foty RA, Shafrir Y and Steinberg MS (1998) Viscoelastic properties of living embryonic tissues: a quantitative study. *Biophysical Journal* **74**:2227.
18. Ranft J *et al.* (2010) Fluidization of tissues by cell division and apoptosis. *Proceedings of the National Academy of Sciences* **107**:20863.
19. Alberts B, Johnson A, Lewis J, Raff M, Roberts K and Walter P, *Molecular Biology of the Cell* (Garland, New York, 2002).
20. Day RE *et al.* (2014) Human aquaporins: regulators of transcellular water flow. *Biochimica et Biophysica Acta* **1840**:1492.
21. Verkman AS, Anderson MO and Papadopoulos MC (2014) Aquaporins: important but elusive drug targets. *Nature Reviews Drug Discovery* **13**: 259.
22. Zetterberg A, Engstrom W and Dafgird E (1984) The relative effects of different types of growth factors on DNA replication, mitosis, and cellular enlargement. *Cytometry* **5**(4):368-375.
23. Reuss L, Cassel D, Rothenberg P, Whitele B, Mancuso D and Glaser L (1986) Mitogens and ion fluxes. In *Current topics in membranes and transport* (Vol. 27, pp. 3-54). Academic Press.
24. Korchev YE, Gorelik J, Lab MJ, Sviderskaya EV, Johnston CL, Coombes CR, Vodyanoy I and Edwards CR (2000) Cell Volume Measurement Using Scanning Ion Conductance Microscopy. *Biophysical Journal* **78**:451-457.
25. Smith JC (1981) Growth factors and pattern formation. *Development* **65**:187-207.
26. Ulloa F and Briscoe J (2007) Morphogens and the control of cell proliferation and patterning in the spinal cord. *Cell Cycle* **6**: 2640.
27. Ginzberg MB, Kafri R and Kirschner M (2015) On being the right (cell) size. *Science* **348**(6236):1245075.
28. Bryant SV and Gardiner DM (2016) The relationship between growth and pattern formation. *Regeneration* **3**:103.
29. Biot MA (1941) General theory of three dimensional consolidation. *Journal of Applied Physics* **12**:155.
30. Biot MA (1956) General solutions of the equations of elasticity and consolidation for a porous material. *Journal of Applied Mechanics* **78**:91.
31. Ambrosi D, Pezzuto D, Riccobelli D, Stylianopoulos T and Ciarletta P (2017) Solid tumors are poroelastic solids with a chemo-mechanical feedback on growth. *Journal of Elasticity* **129**:107.
32. Fraldi M and Carotenuto A (2018) Cells competition in tumor growth poroelasticity *Journal of the Mechanics and Physics of Solids* **112**:345.
33. Gierer A and Meinhardt (1972) A theory of biological pattern formation. *Kybernetik* **12**:30-39.
34. Meinhardt H and Gierer A (1972) Applications of a theory of biological pattern formation based on lateral inhibition. *Journal of Cell Science* **15**:321-346.
35. Meinhardt H (2012) Turing's theory of morphogenesis of 1952 and the subsequent discovery of the crucial role of local self-enhancement and long-range inhibition. *Interface Focus* **2**:407-416.
36. Jiang H and Sun SX (2013) Cellular pressure and volume regulation and implications for cell mechanics. *Biophysical Journal* **105**:609-619.
37. Smith CB and Betz WJ (1996) Simultaneous independent measurement of endocytosis and exocytosis. *Nature* **380**(6574):

38. Bois JS, Julicher F and Grill SW (2011) Pattern formation in active fluids. *Physical Review Letters* **106**:028103.
39. Murray JD, *Mathematical Biology* (Springer-Verlag, Berlin, 2003), third edition.
40. Madzvamuse A, Ndakwo HS and Barreira R (2015) Cross-diffusion-driven instability for reaction-diffusion systems. *Journal of Mathematical Biology* **70**(4):709-743.
41. Vanag VK and Epstein IR (2009) Cross-diffusion and pattern formation in reaction-diffusion systems. *Physical Chemistry Chemical Physics* **11**:897-912.
42. Perthame B, *Transport Equations in Biology* (Springer, Berlin, 2006), first edition.
43. Recho P, Putelat T and Truskinovsky L (2015) Mechanics of motility initiation and motility arrest in crawling cells. *Journal of the Mechanics and Physics of Solids* **84**:469-505.
44. Doedel EJ *et al.* (2007) AUTO-07P: Continuation and bifurcation software for ordinary differential equations.
45. Inomata H, Shibata T, Haraguchi T and Sasai Y (2013) Scaling of dorsal-ventral patterning by embryo size-dependent degradation of Spemann's organizer signals. *Cell* **153**(6):1296-311.
46. Stuckemann T *et al.* (2017) Antagonistic self-organizing patterning systems control maintenance and regeneration of the anteroposterior axis in planarians. *Developmental Cell* **40**(3):248-263.
47. Müller P *et al.* (2012) Differential diffusivity of Nodal and Lefty underlies a reaction-diffusion patterning system. *Science* **336**(6082):721-724.
48. Loren N *et al.* (2015) Fluorescence recovery after photobleaching in material and life sciences: putting theory into practice. *Quarterly Reviews of Biophysics* **48**(3):323-387.
49. Kicheva A, Bollenbach T, Wartlick O, Julicher F and Gonzalez-Gaitan M (2012) Investigating the principles of morphogen gradient formation: from tissues to cells. *Current Opinion in Genetics & Development* **22**(6):527-532.
50. Bläßle A *et al.* (2018) Quantitative diffusion measurements using the open-source software PyFRAP. *Nature Communications* **9**(1):1582.
51. Crank J, *The Mathematics Of Diffusion* (Oxford University Press, Oxford, 1979), first edition.
52. Hashin Z and Shtrikman S (1962) A variational approach to the theory of the effective magnetic permeability of multiphase materials. *Journal of applied Physics* **33**(10):3125-3131.
53. P. Muller, K. W. Rogers, S. R. Yu, M. Brand and A. F. Schier (2013) Morphogen transport. *Development* **140**:1621-1638.
54. Freund JB, Goetz JG, Hill KL and Vermot J (2012) Fluid flows and forces in development: functions, features and biophysical principles. *Development* **139**(7):1229-1245.
55. Coussy O, *Poromechanics* (Wiley, London, 2004), first edition.
56. Heisenberg C-P and Bellaiche Y (2013) Forces in tissue morphogenesis and patterning. *Cell* **153**(5):948-962.
57. He B, Doubrovinski K, Polyakov O and Wieschaus E (2012) Apical constriction drives tissue-scale hydrodynamic flow to mediate cell elongation. *Nature* **508**(7496):392-396.
58. Boehm *et al.* (2010) The role of spatially controlled cell proliferation in limb bud morphogenesis. *PLoS biology* **8**(7):e1000420.
59. Gros J, Hu JKH, Vinegoni C, Feruglio PF, Weissleder R and Tabin CJ (2010) WNT5A/JNK and FGF/MAPK pathways regulate the cellular events shaping the vertebrate limb bud. *Current Biology* **20**(22):1993-2002.
60. Charron F, Stein E, Jeong J, McMahon AP and Tessier-Lavigne M (2003) The morphogen sonic hedgehog is an axonal chemoattractant that collaborates with netrin-1 in midline axon guidance. *Cell* **113**(1):11-23.
61. Hodges A, Alan Turing: *The Enigma* (Princeton University Press, Princeton, 2014), new edition.
62. Copeland BJ, Turing: *Pioneer of the information age* (OUP, Oxford, 2014), first edition.
63. Turing AM (1952) The chemical basis of morphogenesis. *Philosophical Transactions of the Royal Society B: Biological Sciences* **237**(641):37-72.
64. Smith JM, *Shaping life: genes, embryos and evolution.* (Yale University Press, New Haven, 1999), first edition.
65. Wolpert L (1969) Positional information and the spatial pattern of cellular differentiation. *Journal of Theoretical Biology* **25**(1):1-47.
66. Prigogine I and Nicolis G (1967) On symmetry-breaking instabilities in dissipative systems. *Journal of Chemical Physics* **46**(9):3542-3550.
67. Crick F (1970) Diffusion in Embryogenesis. *Nature* **225**(1):420-422.
68. Othmer HG and Scriven LE (1969) Interactions of reaction and diffusion in open systems. *Industrial and Engineering Chemistry Fundamentals* **8**(2):302-313.
69. AMT/D/5, Alan Turing Archive, King's College Archive Centre, Cambridge (UK).
70. Othmer HG and Scriven LE (1971) Instability and dynamic pattern in cellular networks. *Journal of Theoretical Biology* **32**(3):507-537.
71. Othmer HG (1977) Current problems in pattern formation. *Lectures on Mathematics in the Life Science* **9**:57-85.
72. Finlayson BA and Scriven LE (1969) Convective instability by active stress. *Proceedings of the Royal Society A: Mathematical, Physical and Engineering Sciences* **310**(1501):183-219.
73. Oster GF, Murray JD and Harris AK (1983) Mechanical aspects of mesenchymal morphogenesis. *Development* **78**(1):83-125.